Visualization of Alternating Triangular Domains of Charge Density Waves in $2H$-NbSe$_2$ by Scanning Tunneling Microscopy

Shunsuke Yoshizawa[1,*] Keisuke Sagisaka,[1] and Hideaki Sakata[2]

[1]*Center for Basic Research on Materials, National Institute for Materials Science, 1-2-1 Sengen, Tsukuba, Ibaraki 305-0047, Japan*
[2]*Department of Physics, Tokyo University of Science, 1-3 Kagurazaka, Shinjuku, Tokyo 162-8601, Japan*

The charge density wave (CDW) state of $2H$-NbSe$_2$ features commensurate domains separated by domain boundaries accompanied by phase slips known as discommensurations. We have unambiguously visualized the structure of CDW domains using a displacement-field measurement algorithm on a scanning tunneling microscopy image. Each CDW domain is delimited by three vertices and three edges of discommensurations and is designated by a triplet of integers whose sum identifies the types of commensurate structure. The observed structure is consistent with the alternating triangular tiling pattern predicted by a phenomenological Landau theory. The domain shape is affected by crystal defects and also by topological defects in the CDW phase factor. Our results provide a foundation for a complete understanding of the CDW state and its relation to the superconducting state.

The charge density wave (CDW) is a cooperative phenomenon characteristic of low-dimensional metals [1,2]. CDWs that coexist with other ordered states, exemplified by superconductivity, are of particular interest in view of the interplay between multiple orders [3]. Notable examples are CDWs in cuprate superconductors [4,5], kagome superconductors [6,7], and transition metal dichalcogenides (TMDCs) [8]. $2H$-NbSe$_2$ is a prototypical TMDC that exhibits both the CDW and superconducting states. It undergoes a triple-Q CDW transition, where three equivalent CDW wave vectors are 120° apart, at a temperature of $T_{\mathrm{CDW}} \sim 30$ K. Although neutron and x-ray diffraction experiments indicate an incommensurate periodicity [9,10], scanning tunneling microscopy (STM) studies have unveiled locally 3×3 commensurate domains [11–16]. Domain boundaries serve as discommensurations, where the phase of the CDW shifts over a short distance [17]. Superconductivity occurs below the critical temperature of $T_c \sim 7$ K. A recent STM study [18] reveals the existence of the Cooper-pair density wave state, which shares the same periodicity as the CDW with a constant phase difference. These two modulated states have a common domain boundary. The results of another study [19] imply that the superconductivity competes with the CDW depending on the commensurate local structure. To better understand the interplay between the CDW and superconductivity, precise knowledge of the domain structure of the CDW is indispensable.

Despite extensive study, the domain structure of the CDW of $2H$-NbSe$_2$ remains elusive. As shown in Fig. 1(a), the crystal structure of $2H$-NbSe$_2$ consists of Nb atoms forming a triangular lattice and Se atoms protruding up and down from the Nb plane. STM observations and density functional theory calculations have identified two types of commensurate domain with distinct local structures [15,19,20]. One is characterized by the CDW maxima at Se sites, referred to as the chalcogen-centered (CC) structure. The other is characterized by the CDW maxima at hollow sites and is referred to as the hollow-centered (HC) structure. Gye *et al.* have proposed a complex structure of these CDW domains [15], where HC domains are classified into nine types depending on the phase of modulation, forming isolated hexagonal patches, and CC domains surround HC domains and form a honeycomb network. However, Gye *et al.* did not provide a nonvisual method to identify the domain boundary. Furthermore, they focused on the domain of only the HC structure and treated the CC structure as a type of discommensuration. This asymmetric treatment of the two commensurate structures and the ambiguity in domain identification may have prevented a simpler understanding of the domain structure. Other groups reported the detection of discommensurations as steep changes in the phase factor of the CDW extracted from topographic images [18,21], but the nonvisual determination of the shape and the type of domains remained unresolved.

Here, we present a systematic approach to visualize the CDW domain structure of $2H$-NbSe$_2$ using topographic images obtained by STM. Through a simple simulation, we demonstrate that the local CDW structure is characterized by a triplet of real numbers, denoted as (n_1, n_2, n_3). In each commensurate domain, the triplet takes integer values and their sum modulo 3 determines the type of commensurate structure. We determined the spatial variation of (n_1, n_2, n_3) by measuring the displacement fields of the CDW modulations relative to the atomic lattice in a
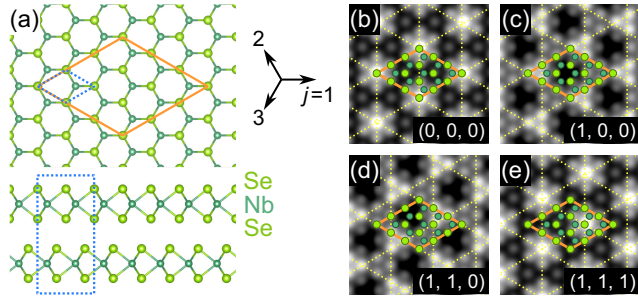
FIG. 1. (a) Top view (upper panel) and front view (lower panel) of the crystal structure of $2H$-NbSe$_2$ [22]. The unit cell is depicted by a dotted rhombus (top view) and a dotted rectangle (front view). The solid rhombus indicates the 3×3 unit cell of the commensurate CDW. (b)–(e) Simulated CDW images with several combinations of indices (n_1, n_2, n_3). The dotted lines indicate the maxima of CDW components. The solid rhombus indicates the 3×3 unit cell of the CDW and is fixed to the atomic lattice to show the relative position of the CDW maxima.

topographic image, thereby revealing the domain structure without relying on visual interpretation. Each CDW domain is bounded by three vertices and three edges, consistent with the alternating triangular tiling predicted by an empirical Landau theory. The deformation of the domain shape from an equilateral triangle is attributed to the pinning of discommensurations by crystalline defects.

We used an ultrahigh-vacuum (UHV) cryogenic STM system based on the model USM-1300 from Unisoku Co. Ltd. The STM tip was fabricated by focused ion beam from a mechanically sharpened Pt-Ir wire and conditioned on a clean Au(111) surface prior to the experiment. The single-crystal $2H$-NbSe$_2$ was grown by the chemical vapor transport method using iodine as the transport agent. The sample was cleaved in UHV at room temperature and immediately transferred to the STM head kept at a low temperature. All the STM data presented in this Letter were recorded in a constant-current mode at 4.5 K in zero magnetic field. The resistivity measurement of a sample in the same batch gives the residual resistivity ratio of 42, $T_c = 7.3$ K, and $T_{\mathrm{CDW}} \simeq 30$ K.

Figure 2(a) shows a high-resolution topographic image of a 100 nm $\times$ 100 nm area that clearly resolves the CDW modulations as well as the triangular lattice of Se atoms. The image also displays several types of atomic-scale defect. The Fourier transform of this image [Fig. 2(b)] displays sharp peaks at the periodicity of the crystal lattice ($\mathbf{b}_1$, $\mathbf{b}_2$, and $\mathbf{b}_3$) and slightly broader peaks at the periodicity of the CDW ($\mathbf{Q}_1$, $\mathbf{Q}_2$, and $\mathbf{Q}_3$). The broad nature of the latter peaks reflects the finite size of CDW domains. All the other peaks are considered as harmonics of these periodicities. The line profiles in Fig. 2(c) indicate that the length of $\mathbf{Q}_j$ is approximately one-third that of $\mathbf{b}_j$. Upon closer examination of the topographic image, we observe a difference in local atomic-scale structure. Figures 2(d) and 2(e) depict enlarged images cropped from
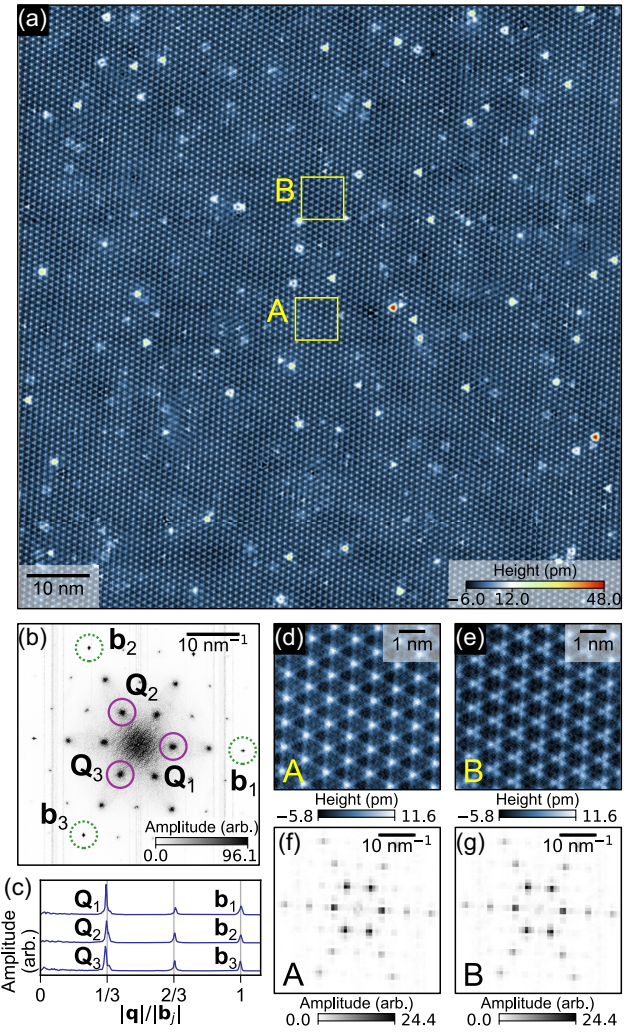

FIG. 2. (a) Topographic image of a 100 nm $\times$ 100 nm area of a cleaved surface of $2H$-NbSe$_2$. The data were recorded at a resolution of 2048×2048 but were resampled to 1024×1024 to reduce the file size. The image was flattened by subtracting a third-order polynomial fit from each line. The feedback condition was 500 pA at 50 mV. (b) Fourier transform of the topographic image in (a). The dotted and solid circles indicate the spots of the atomic lattice ($\mathbf{b}_1$, $\mathbf{b}_2$, and $\mathbf{b}_3$) and those of the CDW ($\mathbf{Q}_1$, $\mathbf{Q}_2$, and $\mathbf{Q}_3$), respectively. (c) Line profiles of the Fourier transform image along $\mathbf{b}_1$, $\mathbf{b}_2$, and $\mathbf{b}_3$ directions. (d) and (e) Cropped images of the CC and HC domains indicated by the boxes labeled A and B in (a). (f) and (g) Fourier transform images of cropped data of (d) and (e).

the regions labeled A and B in Fig. 2(a), respectively. The former displays a repeated star-shaped pattern that is characteristic of the CC structure, while the latter displays a repeated clover-shaped pattern of the HC structure [15,19]. Figures 2(f) and 2(g) show the corresponding Fourier transforms. The patterns are almost identical to each other at the pixel level. This indicates that the CC and HC structures share the same periodic components but differ in their phase.

To investigate how the relative phase alters the topographic appearance, we present a simple simulation. We approximate the charge density within a commensurate domain by the sum of two functions of position $\mathbf{r} = (x, y)$,

$$\rho^{(n_1,n_2,n_3)}(\mathbf{r}) = \rho_{\text{Se}}(\mathbf{r}) + c\rho_{\text{CDW}}^{(n_1,n_2,n_3)}(\mathbf{r}). \quad (1)$$

Here, $\rho_{\text{Se}}(\mathbf{r}) = \text{Re}\sum_{j=1}^{3}\exp(i\mathbf{b}_j \cdot \mathbf{r})$ represents the lattice modulations with maxima at Se sites, and $\rho_{\text{CDW}}^{(n_1,n_2,n_3)}(\mathbf{r}) = \text{Re}\sum_{j=1}^{3}\exp[i(\mathbf{Q}_j \cdot \mathbf{r} - 2\pi n_j/3)]$ provides the CDW modulations with commensurate wave vectors $\mathbf{Q}_j = (1/3)\mathbf{b}_j$. The indices $j = 1, 2, 3$ represent the directions. The constant c controls the amplitude of the CDW modulations relative to the lattice modulations, and we set it to be ~ 2.5. The CDW modulations have phase offsets controlled by n_j. Increasing n_j by 1 translates the jth component of the CDW by a lattice constant, and increasing it by 3 restores the CDW to its initial position. The simulated topographic images $\rho^{(n_1,n_2,n_3)}(\mathbf{r})$ for several combinations of (n_1, n_2, n_3) are shown in Figs. 1(b)–1(e). In the case of (0,0,0) [Fig. 1(b)], the CDW and the atomic lattice are in phase, and CDW maxima are located at Se sites at the corner of the 3×3 cell. This condition yields a topographic image of the CC structure. In the case of (1,0,0) [Fig. 1(c)], CDW maxima are located at hollow sites, and the image shows the clover-shaped pattern of the HC structure. In the case of (1,1,0) [Fig. 1(d)], CDW maxima are located at Nb sites. The pattern resembles that of the HC structure, but the orientation of the clover is the opposite. In the case of (1,1,1) [Fig. 1(e)], the image again displays the CC structure, but CDW maxima are at Se sites different from those for (0,0,0). By examining the structure of various combinations of (n_1, n_2, n_3) in this manner, we observe that the type of domain is determined by $\lambda \equiv (\sum_{j=1}^{3} n_j)$ mod 3, with $\lambda = 0$ corresponding to the CC structure and $\lambda = 1$ to the HC structure. All the possible structures are presented in Sec. S1 of Supplemental Material (SM) [23].

The precise determination of the triplet (n_1, n_2, n_3) from the topographic image is essential for visualizing the domain structure. To achieve this, we utilize a displacement detection algorithm proposed by Lawler and Fujita et al. [26]. Assuming that the topographic image $z(\mathbf{r})$ contains a CDW modulation with periodicity $\mathbf{Q}_j$ that is altered by a slowly varying displacement field $\mathbf{u}_j(\mathbf{r})$, we obtain the displacement field using the relation

$$\exp[-i\mathbf{Q}_j \cdot \mathbf{u}_j(\mathbf{r})] \propto \sum_{\mathbf{r}'} z(\mathbf{r}') \exp(-i\mathbf{Q}_j \cdot \mathbf{r}') w(\mathbf{r} - \mathbf{r}'), \quad (2)$$

where $w(\mathbf{r}) = (2\pi\sigma^2)^{-1}\exp[-|\mathbf{r}|^2/(2\sigma^2)]$ is a two-dimensional Gaussian with a spatial extent of σ. We set $\sigma = 1$ nm in the present analysis. From the phase component of the right-hand side, we obtain the (apparent) displacement field $u_j(\mathbf{r}) \equiv \mathbf{u}_j(\mathbf{r}) \cdot \mathbf{Q}_j/|\mathbf{Q}_j|$ for each j.

However, this quantity includes an extrinsic image deformation $\mathbf{v}(\mathbf{r})$, which originates from the creep effect of the piezoelectric scanner or the drift of the sample. To eliminate this extrinsic effect, we extract $\mathbf{v}(\mathbf{r})$ by applying the Lawler-Fujita algorithm to the periodicities $\mathbf{b}_j$ of the crystal lattice. We then obtain the intrinsic displacement fields of the CDW modulations by subtracting $v_j(\mathbf{r}) \equiv \mathbf{v}(\mathbf{r}) \cdot \mathbf{b}_j/|\mathbf{b}_j|$ from $u_j(\mathbf{r})$. These intrinsic displacement fields are then divided by the interplanar spacing to obtain the spatial dependences of (n_1, n_2, n_3). A complete description of this procedure is presented in Sec. S2 of SM [23].

Figures 3(a)–3(c) show the images of $n_1(\mathbf{r})$, $n_2(\mathbf{r})$, and $n_3(\mathbf{r})$ determined from the topographic image in Fig. 2(a). Each image displays a step-terrace structure, and the histograms in Figs. 3(d)–3(f) show sharp peaks at integer values, highlighting the successful determination of n_j values. The results also show that the region is mostly covered by commensurate domains. The domain structure was visualized in Fig. 3(g) by plotting $\lambda(\mathbf{r}) \equiv \{\sum_j \text{nint}[n_j(\mathbf{r})]\}$ mod 3, where nint denotes the nearest integer. The region is composed of alternating domains of $\lambda = 0$ (CC) and $\lambda = 1$ (HC), along with small areas with $\lambda = 2$ at the intersections of domain boundaries. Each domain is enclosed by three vertices and three edges and is identified by a unique triplet of integers (n_1, n_2, n_3). The realization of this domain structure indicates that the discommensurations of the $\mathbf{Q}_1$, $\mathbf{Q}_2$, and $\mathbf{Q}_3$ components are not independent but are forced to intersect at a single vertex. A direct comparison of the domain structure and the topographic image is shown in Fig. S7 of SM [23]. We have confirmed the reproducibility of the present findings on another $2H$-NbSe$_2$ sample (see Sec. S4 of SM [23]).

We also evaluated the width of the discommensurations. For each j, we defined the discommensurate region as the region where $n_j(\mathbf{r})$ is closer to a half-integer than to an integer. We then estimated the width by dividing the area of the discommensurate region by the total length of the discommensuration. Details are provided in Sec. S3 of SM [23]. The estimated width was about 3 nm for all CDW components. This is not an artifact but the real width of the discommensuration, because the value is larger than the broadening induced by the σ of the Gaussian function $w(\mathbf{r})$. This finding implies why Gye et al. [15] proposed a picture different from ours, where the HC domains were suggested to form isolated patches separated by continuous CC regions. This interpretation arises when the discommensurate region in our definition is misassigned to the CC region.

The domain structure revealed here is consistent with the results of the studies based on the phenomenological Landau theory in the 1970s–1980s [17,27–29]. In particular, McMillan's theory of discommensuration [17] was extended to describe the CDW states of TMDCs with a focus on $2H$-TaSe$_2$ [27–29]. These studies classified three possible commensurate structures, depending on the
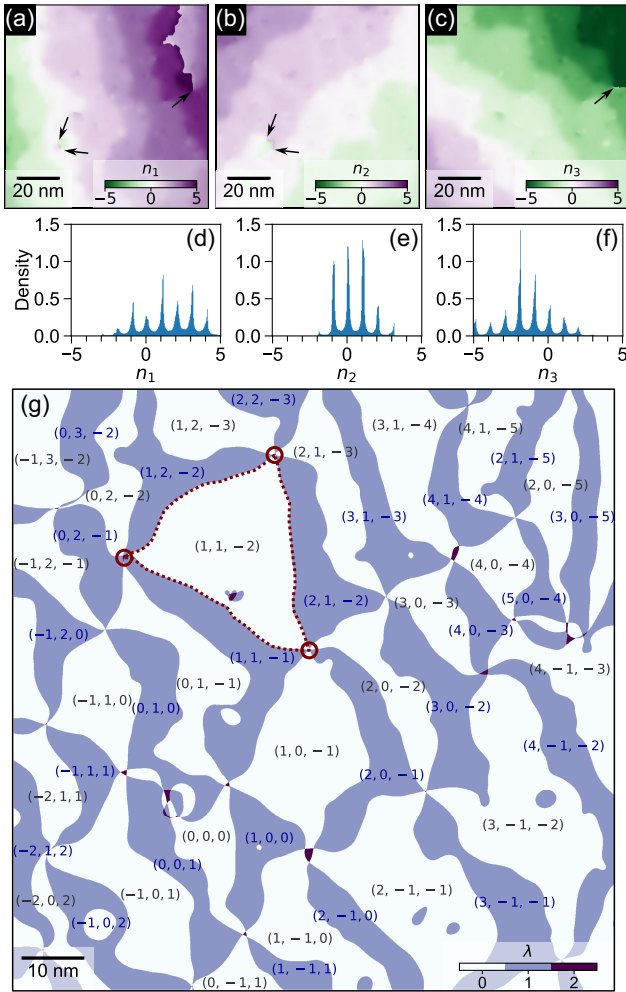
FIG. 3. (a)–(c) Images of $n_1(\mathbf{r})$, $n_2(\mathbf{r})$, and $n_3(\mathbf{r})$. The arrows indicate the locations of topological defects. (d)–(f) Histograms of $n_1(\mathbf{r})$, $n_2(\mathbf{r})$, and $n_3(\mathbf{r})$. (g) Image of $\lambda(\mathbf{r})$. The CC and HC domains are depicted as white and blue areas, respectively. A triplet (n_1, n_2, n_3) is written in each domain. The circles and dotted curves are the vertices and edges of the $(0, 1, -1)$ CC domain, respectively.

location of the threefold rotation axis, and showed that these structures were labeled by three integers, as we have found in our analysis. Nakanishi and Shiba [28,29] proposed a generic form of the free energy with many parameters and performed a numerical minimization for a parameter set that gives the situation where two types of commensurate structure become equally stable. They predicted an alternating triangular tiling pattern of the two types of commensurate domain [29]. Figure 4(a) shows the CDW image simulated by minimizing Nakanishi-Shiba's free energy. Details of the numerical simulation are shown in Sec. S5 of SM [23]. Although the parameter choice was not optimized to describe 2H-NbSe$_2$, the predicted pattern is essentially equivalent to the domain structure obtained in our experiment. Note that the theoretical model was proposed before STM began to be used to observe
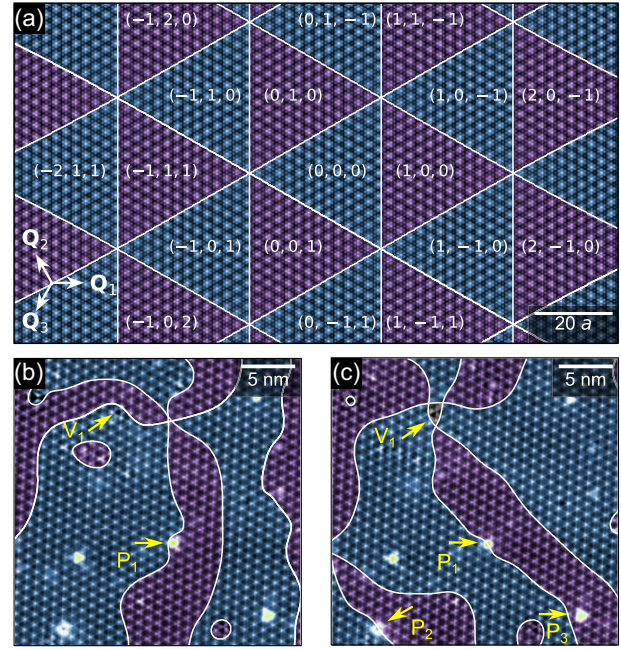

FIG. 4. (a) Simulated topographic image of a $160a \times 90a$ region (a is the lattice constant). (b) Topographic image of a 25 nm $\times$ 25 nm region recorded after the initial cooling from room temperature to 4.5 K. (c) Topographic image of the same region recorded after thermal cycles across T_{CDW}. The white curves represent the discommensurations. The feedback condition was 500 pA at 50 mV. The CC and HC domains are displayed in different colors for clarity.

CDWs [30], and it took nearly 40 years for its direct verification in actual material.

The observed domain structure is heavily deformed compared with the predicted equilateral triangles. This deformation is attributed to the pinning of discommensurations by defects in the crystal, as discussed in theoretical studies [31,32]. Figures 4(b) and 4(c) show the topography of the same region at 4.5 K before and after a thermal cycle across T_{CDW}. The thermal cycling has significantly altered the domain structure. Before the thermal cycle, a protruding defect P_1 was located on a discommensuration. After the thermal cycle, P_1 and P_2 were on discommensurations and P_3 was also close to a discommensuration. This observation indicates that these protruding defects potentially act as pinning centers. It is reasonable that only some of the defects pin discommensurations, because the present sample surface has a large defect density compared with the spacing between discommensurations. A voidlike defect V_1 also appears to pin discommensurations. The exact roles of the different types of defect remain unclear in the present study. In addition, it is still uncertain why defects locally induce CDW above T_{CDW} [16,33], but attract discommensurations below T_{CDW}. Although elucidating these points is beyond the scope of this study, our domain visualization method should be crucial for such investigations.

The changes in the domain structure induced by thermal cycling suggest that the observed domain structures correspond to metastable states even at 4.5 K. Smooth relaxation to the ground state was probably prevented by the presence of topological defects, as the density of topological defects depends on the cooling rate [34], a parameter not controlled in this study. Topological defects in the CDW state of $2H$-NbSe$_2$ are known to be excited as vortex-antivortex pairs in the phase factor of the CDW [21,35]. In our case, vortices and antivortices exist at the terminations of the discontinuities in the image of $n_1(\mathbf{r})$ [Fig. 3(a)]. Interestingly, we find that topological defects also exist in $n_2(\mathbf{r})$ and $n_3(\mathbf{r})$ at the same locations as those in $n_1(\mathbf{r})$ [Figs. 3(b) and 3(c)]. This highlights the fact that the topological defects in this system cannot exist independently in a single CDW component, but always appear as vortex-antivortex pairs in any two of the three components. This can prevent $\sum_j n_j$ from changing by more than one around the vortex, thereby avoiding the formation of a region with $\lambda = 2$. Owing to this intertwined nature of the three CDW components, vortex-antivortex pairs of each CDW component cannot annihilate independently but must do so simultaneously. This restriction may hinder the relaxation to the ground-state domain structure free of topological defects.

In conclusion, our low-temperature STM observations, combined with systematic data analysis, have provided an accurate depiction of the domain structure of the CDW state in $2H$-NbSe$_2$. Our findings reveal that each CDW domain is characterized by a triplet of integers, and the domains form an alternating triangular tiling that is deformed by the presence of crystalline and topological defects. Our work provides a basis for understanding the CDW transition in $2H$-NbSe$_2$ and other TMDC systems, and prompts further investigation of the interplay between the CDW and superconductivity.

---

*YOSHIZAWA.Shunsuke@nims.go.jp

[1] G. Grüner, The dynamics of charge-density waves, Rev. Mod. Phys. **60**, 1129 (1988).

[2] X. Zhu, Y. Cao, J. Zhang, E. W. Plummer, and J. Guo, Classification of charge density waves based on their nature, Proc. Natl. Acad. Sci. U.S.A. **112**, 2367 (2015).

[3] A. M. Gabovich, A. I. Voitenko, J. F. Annett, and M. Ausloos, Charge- and spin-density-wave superconductors, Supercond. Sci. Technol. **14**, R1 (2001).

[4] J. M. Tranquada, B. J. Sternlieb, J. D. Axe, Y. Nakamura, and S. Uchida, Evidence for stripe correlations of spins and holes in copper oxide superconductors, Nature (London) **375**, 561 (1995).

[5] S. Lee *et al.*, Generic character of charge and spin density waves in superconducting cuprates, Proc. Natl. Acad. Sci. U.S.A. **119**, e2119429119 (2022).

[6] N. N. Wang, K. Y. Chen, Q. W. Yin, Y. N. N. Ma, B. Y. Pan, X. Yang, X. Y. Ji, S. L. Wu, P. F. Shan, S. X. Xu, Z. J. Tu, C. S. Gong, G. T. Liu, G. Li, Y. Uwatoko, X. L. Dong, H. C. Lei, J. P. Sun, and J.-G. Cheng, Competition between charge-density-wave and superconductivity in the kagome metal RbV$_3$Sb$_5$, Phys. Rev. Res. **3**, 043018 (2021).

[7] F. H. Yu, D. H. Ma, W. Z. Zhuo, S. Q. Liu, X. K. Wen, B. Lei, J. J. Ying, and X. H. Chen, Unusual competition of superconductivity and charge-density-wave state in a compressed topological kagome metal, Nat. Commun. **12**, 3645 (2021).

[8] S. Manzeli, D. Ovchinnikov, D. Pasquier, O. V. Yazyev, and A. Kis, 2D transition metal dichalcogenides, Nat. Rev. Mater. **2**, 17033 (2017).

[9] D. E. Moncton, J. D. Axe, and F. J. DiSalvo, Study of superlattice formation in $2H$-NbSe$_2$ and $2H$-TaSe$_2$ by neutron scattering, Phys. Rev. Lett. **34**, 734 (1975).

[10] C.-H. Du, W. J. Lin, Y. Su, B. K. Tanner, P. D. Hatton, D. Casa, B. Keimer, J. P. Hill, C. S. Oglesby, and H. Hohl, X-ray scattering studies of $2H$-NbSe$_2$, a superconductor and charge density wave material, under high external magnetic fields, J. Phys. Condens. Matter **12**, 5361 (2000).

[11] K. Iwaya, T. Hanaguri, A. Koizumi, K. Takaki, A. Maeda, and K. Kitazawa, Electronic state of NbSe$_2$ investigated by STM/STS, Physica (Amsterdam) **329B–333B**, 1598 (2003).

[12] A. Soumyanarayanan, M. M. Yee, Y. He, J. van Wezel, D. J. Rahn, K. Rossnagel, E. W. Hudson, M. R. Norman, and J. E. Hoffman, Quantum phase transition from triangular to stripe charge order in NbSe$_2$, Proc. Natl. Acad. Sci. U.S.A. **110**, 1623 (2013).

[13] U. Chatterjee, J. Zhao, M. Iavarone, R. D. Capua, J. P. Castellan, G. Karapetrov, C. D. Malliakas, M. G. Kanatzidis, H. Claus, J. P. C. Ruff, F. Weber, J. van Wezel, J. C. Campuzano, R. Osborn, M. Randeria, N. Trivedi, M. R. Norman, and S. Rosenkranz, Emergence of coherence in the charge-density wave state of $2H$-NbSe$_2$, Nat. Commun. **6**, 6313 (2015).

[14] B. Guster, C. Rubio-Verdú, R. Robles, J. Zaldívar, P. Dreher, M. Pruneda, J. Á. Silva-Guillén, D.-J. Choi, J. I. Pascual, M. M. Ugeda, P. Ordejón, and E. Canadell, Coexistence of elastic modulations in the charge density wave state of $2H$-NbSe$_2$, Nano Lett. **19**, 3027 (2019).

[15] G. Gye, E. Oh, and H. W. Yeom, Topological landscape of competing charge density waves in $2H$-NbSe$_2$, Phys. Rev. Lett. **122**, 016403 (2019).

[16] E. Oh, G. Gye, and H. W. Yeom, Defect-selective charge-density-wave condensation in $2H$-NbSe$_2$, Phys. Rev. Lett. **125**, 036804 (2020).

[17] W. L. McMillan, Theory of discommensurations and the commensurate-incommensurate charge-density-wave phase transition, Phys. Rev. B **14**, 1496 (1976).

[18] X. Liu, Y. X. Chong, R. Sharma, and J. C. S. Davis, Discovery of a Cooper-pair density wave state in a transition-metal dichalcogenide, Science **372**, 1447 (2021).

[19] A. Sanna, C. Pellegrini, E. Liebhaber, K. Rossnagel, K. J. Franke, and E. K. U. Gross, Real-space anisotropy of the

superconducting gap in the charge-density wave material 2H-NbSe$_2$, npj Quantum Mater. **7,** 6 (2022).

[20] C.-S. Lian, C. Si, and W. Duan, Unveiling charge-density wave, superconductivity, and their competitive nature in two-dimensional NbSe$_2$, Nano Lett. **18,** 2924 (2018).

[21] Á. Pásztor, A. Scarfato, M. Spera, C. Barreteau, E. Giannini, and C. Renner, Holographic imaging of the complex charge density wave order parameter, Phys. Rev. Res. **1,** 033114 (2019).

[22] K. Momma and F. Izumi, VESTA3 for three-dimensional visualization of crystal, volumetric and morphology data, J. Appl. Crystallogr. **44,** 1272 (2011).

[23] See Supplemental Material at http://link.aps.org/supplemental/10.1103/PhysRevLett.132.056401, which includes Refs. [24,25], for the list of commensurate CDW structures, the detailed procedure for determining CDW domains, the analysis of discommensurate region, a reproducibility check, and details of the numerical simulation.

[24] A. J. Bray, Theory of phase-ordering kinetics, Adv. Phys. **51,** 481 (2002).

[25] S. Vogelgesang, G. Storeck, J. G. Horstmann, T. Diekmann, M. Sivis, S. Schramm, K. Rossnagel, S. Schäfer, and C. Roper, Phase ordering of charge density waves traced by ultrafast low-energy electron diffraction, Nat. Phys. **14,** 184 (2017).

[26] M. J. Lawler, K. Fujita, J. Lee, A. R. Schmidt, Y. Kohsaka, C. K. Kim, H. Eisaki, S. Uchida, J. C. Davis, J. P. Sethna, and E.-A. Kim, Intra-unit-cell electronic nematicity of the high-T_c copper-oxide pseudogap states, Nature (London) **466,** 347 (2010).

[27] M. B. Walker and A. E. Jacobs, Distinct commensurate charge-density-wave phases in the 2H-NbSe$_2$, Phys. Rev. B **24,** 6770 (1981).

[28] K. Nakanishi and H. Shiba, Theory of discommensurations and re-entrant lock-in transition in the charge-density-wave state of 2H-TaSe$_2$, J. Phys. Soc. Jpn. **52,** 1278 (1983).

[29] H. Shiba and K. Nakanishi, Phenomenological Landau theory of charge density wave phase transitions in layered compounds, in *Structural Phase Transitions in Layered Transition Metal Compounds*, edited by K. Motizuki (Springer, Dordrecht, 1986), pp. 175–266, https://doi.org/10.1007/978-94-009-4576-0_3.

[30] B. Giambattista, A. Johnson, R. V. Coleman, B. Drake, and P. K. Hansma, Charge-density waves observed at 4.2 K by scanning-tunneling microscopy, Phys. Rev. B **37,** 2741 (1988).

[31] K. Nakanishi, Effects of impurity pinning on commensurate charge-density-wave state and incommensurate-commensurate transition, J. Phys. Soc. Jpn. **46,** 1434 (1979).

[32] T. M. Rice, S. Whitehouse, and P. Littlewood, Impurity pinning of discommensurations in charge-density waves, Phys. Rev. B **24,** 2751 (1981).

[33] C. J. Arguello, S. P. Chockalingam, E. P. Rosenthal, L. Zhao, C. Gutiérrez, J. H. Kang, W. C. Chung, R. M. Fernandes, S. Jia, A. J. Millis, R. J. Cava, and A. N. Pasupathy, Visualizing the charge density wave transition in 2H-NbSe$_2$ in real space, Phys. Rev. B **89,** 235115 (2014).

[34] T. Kibble, Phase-transition dynamics in the lab and the universe, Phys. Today **60,** No. 9, 47 (2007).

[35] J. I. Okamoto, C. J. Arguello, E. P. Rosenthal, A. N. Pasupathy, and A. J. Millis, Experimental evidence for a Bragg glass density wave phase in a transition-metal dichalcogenide, Phys. Rev. Lett. **114,** 026802 (2015).